applied optics

Confocal microscopy with a microlens array

YINCHUAN YU,[1] XIANJUN YE,[1,2] AND MATTHEW D. MCCLUSKEY[1,*]

[1]Department of Physics and Astronomy, Washington State University, Pullman, Washington 99164-2814, USA
[2]Department of Anatomy and Structural Biology, Gruss Lipper Biophotonics Center, Albert Einstein College of Medicine, Bronx, New York 10461, USA
*Corresponding author: mattmcc@wsu.edu

Received 18 December 2019; revised 19 February 2020; accepted 24 February 2020; posted 26 February 2020 (Doc. ID 386269); published 25 March 2020

Confocal laser scanning microscopy (CLSM) is a preferred method for obtaining optical images with submicrometer resolution. Replacing the pinhole and detector of a CLSM with a digital camera [charge-coupled device (CCD) or complementary metal oxide semiconductor (CMOS)] has the potential to simplify the design and reduce cost. However, the relatively slow speed of a typical camera results in long scans. To address this issue, in the present investigation a microlens array was used to split the laser beam into 48 beamlets that are focused onto the sample. In essence, 48 pinhole-detector measurements were performed in parallel. Images obtained from the 48 laser spots were stitched together into a final image. © 2020 Optical Society of America

https://doi.org/10.1364/AO.386269

1. INTRODUCTION

Confocal microscopy [1] and multiphoton microscopy [2] are among the most popular imaging modalities because of their superior optical sectioning capability [3]. These microscopies have found their way into a wide range of life science [4–8] and materials science [9–13] applications. The ability to detect single-molecule fluorescence has provided a wealth of information and high-resolution images [14–17]. Multiphoton microscopy, despite its advantages (deeper penetration depth and better signal-to-noise ratio), is expensive due to its requirement of a high-intensity laser source [18]. A basic confocal microscopy system uses a relatively inexpensive continuous-wave laser [19]. However, a precise scanning/de-scanning system is required to guide the emitted light through the pinhole, increasing alignment requirements and cost.

Confocal laser scanning microscopy (CLSM) can operate in fluorescent mode, where the collected light has a longer wavelength than the laser, or reflection mode, where the laser light itself is detected. The microscope in the present study operates in reflection mode. Ye and McCluskey [20,21] proposed a modular CLSM design that uses an off-the-shelf digital camera (CCD or CMOS) to replace the physical pinhole and photomultiplier tube. The confocal microscope, as a popular base platform, can have other functionalities added to expand its versatility. For example, a spectroscopic imaging module enables the scanning confocal microscope to do photoluminescence mapping of two-dimensional nanomaterials [22].

Prior work showed that image moment analysis of properly cropped wide-field images in CCD confocal microscopy can yield comparable performance to conventional confocal microscopy [20], including optical sectioning [23]. Subtractive imaging together with Gaussian fits provide further enhancement to the imaging quality [24]. A major drawback of this method is the fairly slow scanning speed. In this work, we introduce a microlens array (MLA) into the incident beam path. This splits the laser into a grid of beamlets, significantly shortening the scanning time.

MLAs have been used in wavefront sensors [25], light field microscopy [26], multifocal multiphoton microscopy [27], vibrational spectroscopy microscopy [28], and confocal microscopy [29–31]. In our work, the MLA is inserted into the incident beam path as an intermediate optical element of the CMOS confocal system, which uses a standard microscope objective and is (physical) pinhole-free. The entire area of the CMOS array is utilized.

Spinning-disk methods use an array of pinholes, rather than a single pinhole, and a detector records the light intensities from the various pinholes [32]. Favro *et al.* [33] and the Yokogawa Electrical Corporation [34] disclosed a MLA disk coupled to a pinhole array disk in order to improve light collection efficiency. A similar approach to focus light through a pinhole array was described by Hell *et al.* [35]. Our method dispenses with pinholes entirely and is thus distinct from these approaches. The lack of a spinning disk has the potential to reduce cost.

2. EXPERIMENT

The system (Fig. 1) is a modification of the confocal microscope described in Ref. [20]. The apparatus was built with the Thorlabs 30 mm cage system. The light source is a 4.5 mW power, 532 nm wavelength collimated laser. A Keplerian

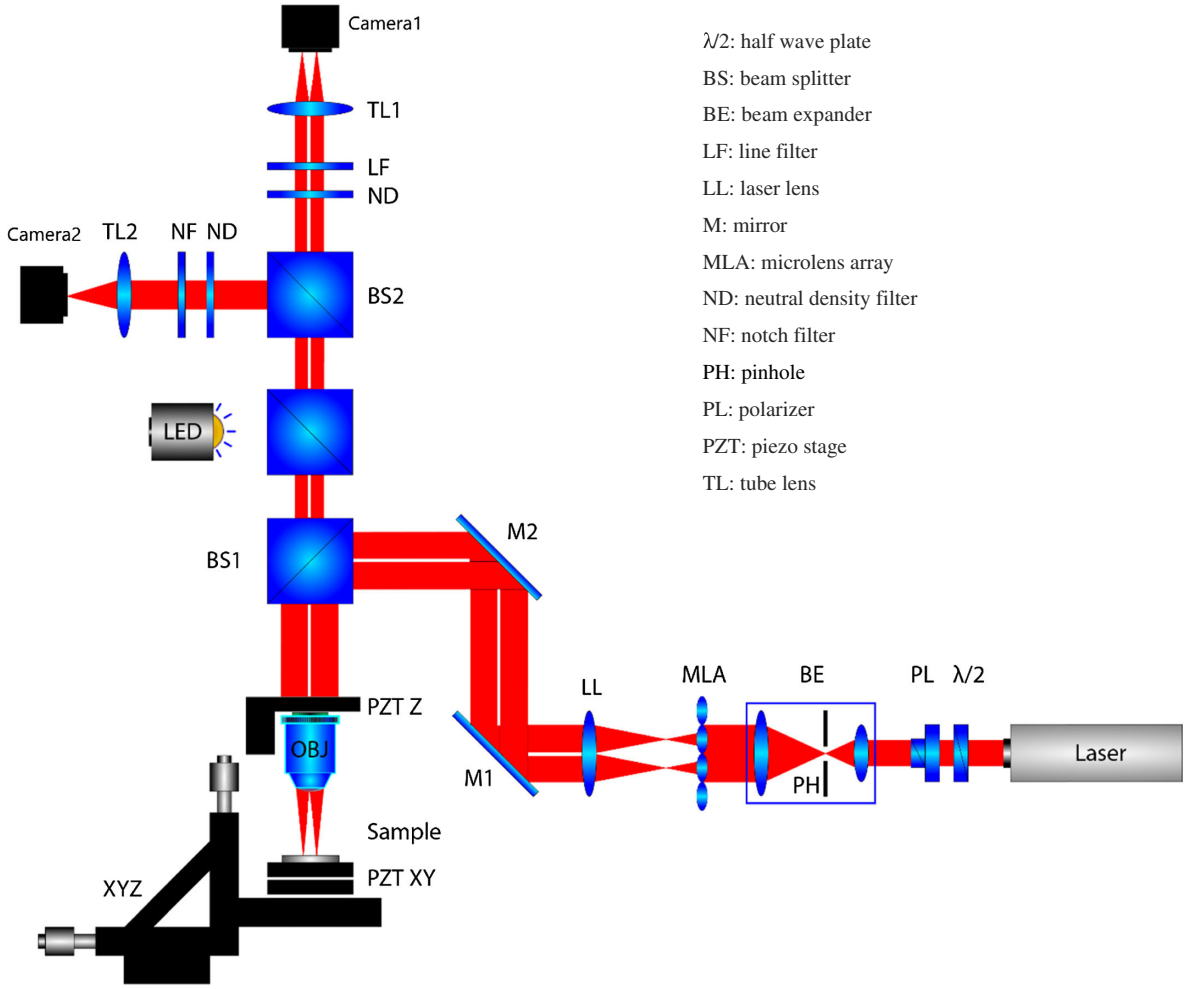

Fig. 1. Schematic diagram of the microscope system. A laser beam passes through the microlens array (MLA) and lens (LL). A beam splitter (BS1) directs the beamlets to the objective lens (OBJ), which focuses them on the sample. Camera2 is a color camera for wide-field microscopy. Along with the light-emitting diode (LED), it is used for sample inspection, i.e., choosing the region of interest. Camera1 is a monochrome camera for acquiring images of reflected laser spots.

style beam expander is placed after the light source to expand the beam in order to overfill the MLA. The MLA (Thorlabs MLA150-5C) consists of a 10 mm × 10 mm square grid of plano-convex lenses on a fused silica substrate. The distance between microlenses, or pitch, is 150 μm, and the focal length of each microlens is 5.6 mm. The MLA splits the beam into a grid of beamlets, and a 200 mm focal length lens is used to collimate these beamlets. The beamlets are then focused on the sample by an 8.2 mm focal length objective lens (20×, numerical aperture = 0.4).

After reflection by the sample, the laser beams are guided by beam splitter cubes into the camera detection module. There are two cameras: an Imaging Source DMK 33UP1300 monochrome camera (Camera1) placed on the vertical arm to collect the reflected laser spots and a DFK 23U274 color camera (Camera2) on the horizontal arm for sample inspection. The sample is moved by the motion module, which contains a piezoelectric position stage controlling the x axis and y axis, a piezoelectric objective scanner controlling the z axis, and a three-axis manual stage for initial position control.

The sample was a US Air Force resolution target (USAF Ready Optics, California, up to group 11). Data acquisition and scanning processes are controlled by a program written in C++. The exposure time was set as 1/500 s, and the scanning step was 0.05 μm. The number of steps was 200 × 200, or 10 μm × 10 μm. On Camera1, an image of 48 reflected laser spots is collected (Fig. 2).

The first step is to find the correct Z position where the sample is in the focal plane of the microscope. This is done by turning on the light-emitting diode (LED), observing the sample with Camera2, and adjusting the objective Z height until the sample surface is in focus. The manual stage is used to select the region of interest. Next, the laser is turned on and the sample is scanned. The scanning time depends on the setting of the camera frequency. In our experiment the frequency was set as 30 frames per second (fps), which resulted in a total scanning time of approximately 20 min.

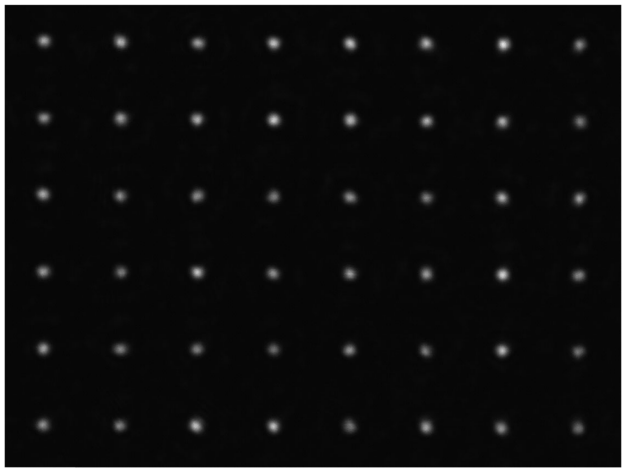

Fig. 2. Reflected laser spots imaged on Camera1.

3. IMAGE PROCESSING

A. Scanning and Image Moment

Before scanning the sample, a high-quality mirror was used to normalize the intensity of each laser spot. The distance between two lenses (pitch) on the MLA is $d_l = 150\ \mu\text{m}$. The distance between two laser spots on the sample is given by

$$d_s = d_l \frac{f_o}{f_l}. \tag{1}$$

Here f_l is the focal length of the laser lens and f_o is the focal length of the objective lens. For $f_l = 200$ mm and $f_o = 8.2$ mm, Eq. (1) yields a distance of $d_s = 6.15\ \mu\text{m}$.

Since the step size is 0.05 μm, we need 123 steps × 123 steps for each laser spot to cover the whole picture. Because some overlap is required for stitching, however, we need to scan additional steps. In practice, 200 steps × 200 steps provide sufficient overlap between adjacent pieces. After scanning, each camera image is cropped evenly into 48 pieces, each of which is 160 pixels × 160 pixels.

The image moment is defined as

$$M_{pq} = \sum_x \sum_y x^p y^q I(x, y), \tag{2}$$

where $I(x, y)$ is the intensity at pixel (x, y). The sum is performed over a 60 pixel × 60 pixel region around the laser spot. From Eq. (2), the zeroth-order image moment M_{00} is the irradiance. By calculating each spot's zeroth-order image moment, 48 200 × 200 matrices, or *graphs*, are formed (Fig. 3).

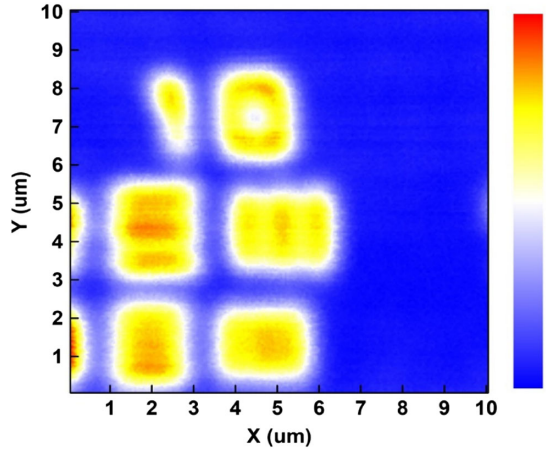

Fig. 3. Graph formed by one of the laser spots. Each pixel on the graph is determined by the value of the zeroth-order image moment. The image shows part of the USAF target group 10.

B. Gaussian Fits

An alternative analysis was performed by fitting the laser spots to Gaussian functions. The equation for a 2D Gaussian is

$$g(x, y) = A \cdot \exp\left(-\frac{(x - \bar{x})^2}{2\sigma_x{}^2} - \frac{(y - \bar{y})^2}{2\sigma_y{}^2}\right), \tag{3}$$

where A is the peak intensity and $(\bar{x}, \bar{y})$ gives the spot's central position. An example of a fit to one laser spot is shown in Fig. 4. The difference between the experimental and simulated images, normalized to the maximum of the experimental image, is shown in Fig. 4(c).

This fit is performed for each step, and the A value (amplitude) is plotted in a graph. Figure 5 shows a graph of the A value of the Gaussian fit for the same scanning region as Fig. 3. Comparing Figs. 3 and 5, it is apparent that the graph of A is sharper than that of M_{00}. A 1D slice of the image is plotted in

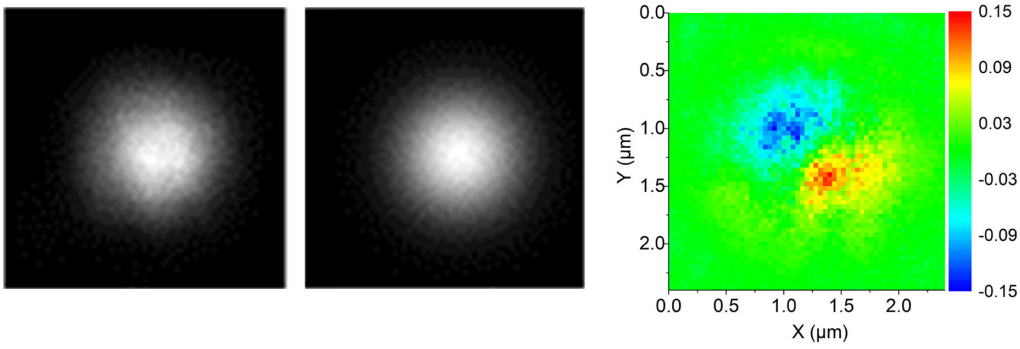

Fig. 4. (a) Laser spot obtained by Camera1. (b) 2D Gaussian fit. (c) False-color image of the normalized difference between the experimental spot and the fit.

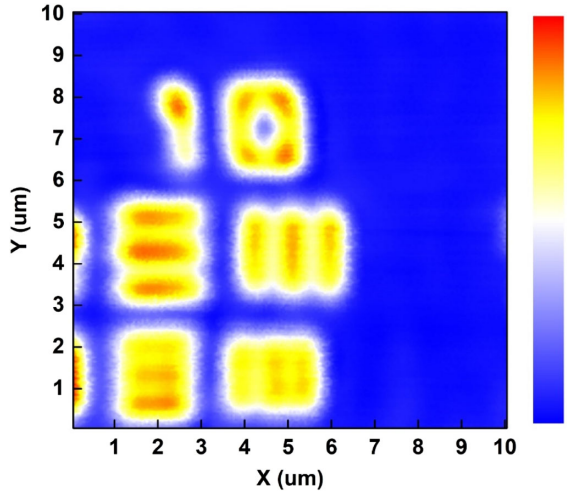

Fig. 5. Graph of the A value of the Gaussian fit. Each pixel on the graph is determined by the A value (amplitude) of a 2D Gaussian function. The scanning region is the same as Fig. 3.

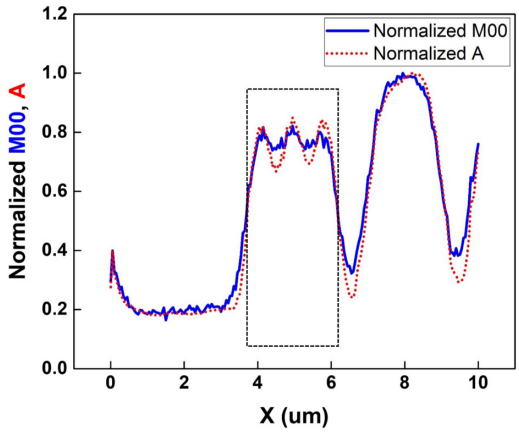

Fig. 6. Comparison of graphs made by the A value of the Gaussian fit and the zeroth-order image moment. The rectangular region is group 10, element 2.

Fig. 6. The highlighted region is the intensity of a line across three stripes from USAF group 10, element 2. These rectangular stripes and the gaps between them are each 0.435 μm wide [36]. A qualitative assessment of Fig. 6 indicates that the plot of the A value has lower noise and higher contrast.

C. Stitching Algorithm

The lenses on the MLA are not perfectly uniform, which causes the laser spots to have position and intensity deviations. Simply combining 48 pieces will cause boundary discontinuities. To correct this artifact, an algorithm was introduced to smoothly join, or *stitch*, the 48 images. Each image was first multiplied by a normalization constant obtained from the mirror scan. For two neighboring pieces, rectangular portions were selected that should overlap (40 pixels × 160 pixels for a vertical boundary, as shown in Fig. 7, and 160 pixels × 40 pixels for a horizontal boundary).

Plotting values of each pixel of one rectangular portion versus the values of the neighbor's portion, a linear regression was constructed [Fig. 8(a)]. The rectangular portion on the neighboring graph was moved until the best linearity was found, which returned a maximized r-squared value [37]. This relative position indicates how the neighboring piece should be translated. The r-squared value itself is a statistical measure of the quality of the linear regression.

Repeating this procedure for the boundaries of all 48 pieces, the whole graph is formed piece by piece, like a puzzle. In order to combine all pieces into a whole graph with minimum discontinuity and highest position accuracy, the piece that yields the highest r-squared value is added first. For example, consider the first piece, which is in the upper-left corner. There are two neighboring pieces, below and to the right. The linear regression procedure is performed for both of these neighboring pieces. Whichever one yields the highest r-squared value is added to the board. This procedure is repeated until the 48th piece is added.

Finally, boundary discontinuities are smoothed by adding a gradient value across a width of 20 pixels. The smoothing equation is

$$I = I_0 + \tfrac{1}{2} D \left(1 - \tfrac{x}{10}\right), \tag{4}$$

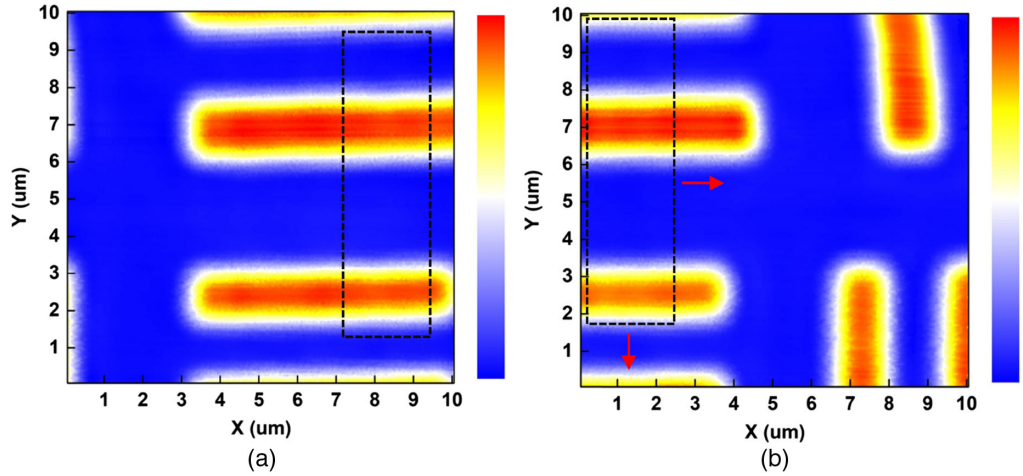

Fig. 7. Rectangular portions on two neighboring pieces. One of the portions is moved until the best overlap is achieved.

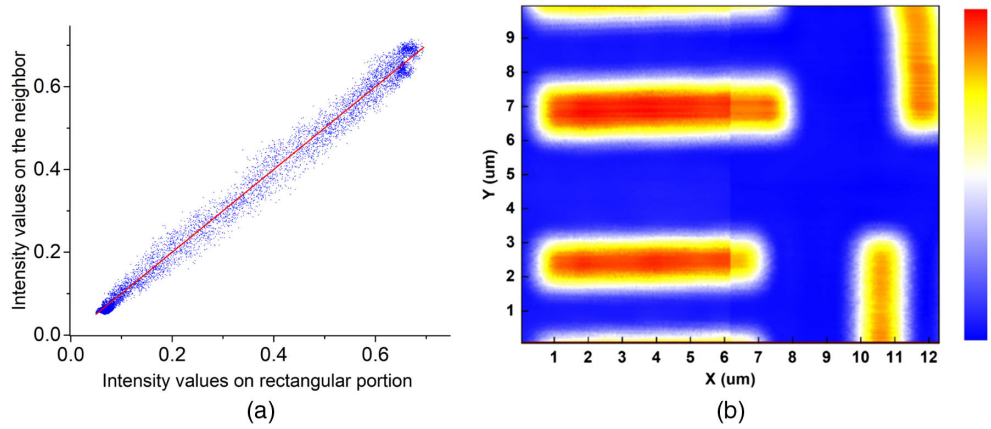

Fig. 8. (a) Linear fit with r-squared value closest to 1. (b) Result of combining the two neighboring pieces based on the result.

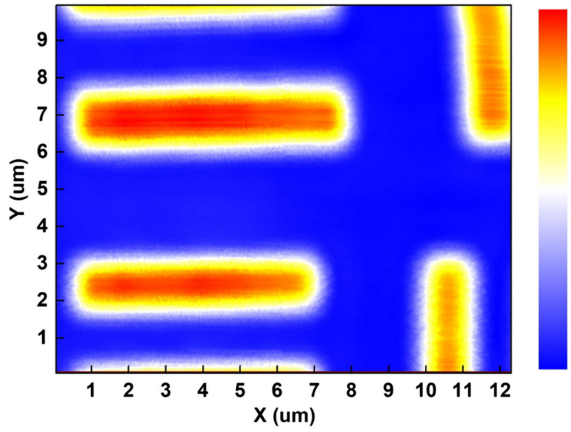

Fig. 9. Same graph as Fig. 8(b), with the boundary smoothed via Eq. (4).

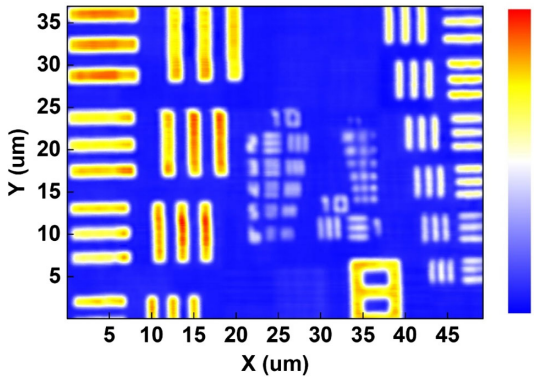

Fig. 10. Whole graph formed by the stitching method.

where I is the adjusted intensity, I_0 is the original intensity, D is the difference between the intensity of two pixels on each side of the boundary, and x is the number of pixels away from the boundary. The graph of Fig. 8(b) after smoothing is shown in Fig. 9. The whole graph is shown in Fig. 10.

4. CONCLUSIONS

We have demonstrated that a MLA confocal microscope produces images with submicrometer spatial resolution. In principle, using a MLA could reduce scanning times arbitrarily, limited only by the camera frame rate and number of laser spots in the field of view. In our experiment, graphs made by Gaussian fits have higher contrast than those obtained using M_{00} (irradiance). Rectangular stripes separated by 0.4 μm can be resolved via the Gaussian-fit method. Stitching methods were used to minimize the boundary discontinuities. This method can be applied to fluorescence microscopy by placing an appropriate filter in front of the camera.

Funding. Directorate for Mathematical and Physical Sciences (DMR-1561419); National Science Foundation.

Disclosures. M. D. M.: Klar Scientific (I,E,P).

REFERENCES

1. M. Minsky, "Memoir on inventing the confocal scanning microscope," Scanning **10**, 128–138 (1988).
2. W. Denk, J. H. Strickler, and W. W. Webb, "Two-photon laser scanning fluorescence microscopy," Science **248**, 73–76 (1990).
3. L. Novotny and B. Hecht, *Principles of Nano-Optics*, 2nd ed. (Cambridge University, 2012).
4. D. J. Stephens and V. J. Allan, "Light microscopy techniques for live cell imaging," Science **300**, 82–86 (2003).
5. P. C. Hickey, S. R. Swift, M. G. Roca, and N. D. Read, "Live-cell imaging of filamentous fungi using vital fluorescent dyes and confocal microscopy," in *Methods in Microbiology*, T. Savidge and P. Charalabos, eds. (Elsevier, 2004), Vol. **34**, pp. 63–87.
6. F. Helmchen and W. Denk, "Deep tissue two-photon microscopy," Nat. Methods **2**, 932–940 (2005).
7. T. G. Phan and A. Bullen, "Practical intravital two-photon microscopy for immunological research: faster, brighter, deeper," Immunol. Cell Biol. **88**, 438–444 (2010).
8. A. Ettinger and T. Wittmann, "Fluorescence live cell imaging," Meth. Cell Biol. **123**, 77–94 (2014).
9. W. Hoheisel, W. Jacobsen, B. Lüttge, and W. Weiner, "Confocal microscopy: applications in materials science," Macromol. Mater. Eng. **286**, 663–668 (2001).
10. D. B. Hovis and A. H. Heuer, "The use of laser scanning confocal microscopy (LSCM) in materials science," J. Microsc. **240**, 173–180 (2010).

11. A. M. Chizhik, R. Jäger, A. I. Chizhik, S. Bär, H.-G. Mack, M. Sackrow, C. Stanciu, A. Lyubimtsev, M. Hanack, and A. J. Meixner, "Optical imaging of excited-state tautomerization in single molecules," Phys. Chem. Chem. Phys. **13**, 1722–1733 (2011).
12. E. S. Barnard, E. T. Hoke, S. T. Connor, J. R. Groves, T. Kuykendall, Z. Yan, E. C. Samulon, E. D. Bourret-Courchesne, S. Aloni, P. J. Schuck, C. H. Peters, and B. E. Hardin, "Probing carrier lifetimes in photovoltaic materials using subsurface two-photon microscopy," Sci. Rep. **3**, 2098 (2013).
13. S. Sadeghi, S. K. Abkenar, C. W. Ow-Yang, and S. Nizamoglu, "Efficient white LEDs using liquid-state magic-sized CdSe quantum dots," Sci. Rep. **9**, 10061 (2019).
14. B. Sick, B. Hecht, and L. Novotny, "Orientational imaging of single molecules by annular illumination," Phys. Rev. Lett. **85**, 4482–4485 (2000).
15. B. Lounis and W. E. Moerner, "Single photons on demand from a single molecule at room temperature," Nature **407**, 491–493 (2000).
16. A. Débarre, R. Jaffiol, C. Julien, D. Nutarelli, A. Richard, P. Tchénio, F. Chaput, and J.-P. Boilot, "Quantitative determination of the 3D dipole orientation of single molecules," Eur. Phys. J. D **28**, 67–77 (2004).
17. S. Boichenko, "Theoretical investigation of confocal microscopy using an elliptically polarized cylindrical vector laser beam: visualization of quantum emitters near interfaces," Phys. Rev. A **97**, 043825 (2018).
18. P. T. So, "Two-photon fluorescence light microscopy," in *Encyclopedia of Life Sciences* (Macmillan, 2002), pp. 1–5.
19. J. Pawley, *Handbook of Biological Confocal Microscopy* (Springer, 2010).
20. X. Ye and M. D. McCluskey, "Modular scanning confocal microscope with digital image processing," PLoS One **11**, e0166212 (2016).
21. M. D. McCluskey, "Digital confocal optical profile microscopy," U.S. patent 9,891,422 (13 February 2018).
22. Q. Wang, L. Yang, S. Zhou, X. Ye, Z. Wang, W. Zhu, M. D. McCluskey, and Y. Gu, "Phase-defined van der WaalsSchottky junctions with significantly enhanced thermoelectric properties," J. Phys. Chem. Lett. **8**, 2887–2894 (2017).
23. E. Sánchez-Ortiga, C. J. R. Sheppard, G. Saavedra, M. Martínez-Corral, A. Doblas, and A. Calatayud, "Subtractive imaging in confocal scanning microscopy using a CCD camera as a detector," Opt. Lett. **37**, 1280–1282 (2012).
24. X. Ye and M. D. McCluskey, "Subtractive imaging using Gaussian fits and image moments in confocal microscopy," Res. J. Opt. Photon. **1**, 1000102 (2017).
25. G. Artzner, "Microlens arrays for Shack-Hartmann wavefront sensors," Opt. Eng. **31**, 1311–1322 (1992).
26. M. Levoy, R. Ng, A. Adams, M. Footer, and M. Horowitz, "Light field microscopy," in *ACM SIGGRAPH* (2006), pp. 924–934.
27. J. Bewersdorf, R. Pick, and S. W. Hell, "Multifocal multiphoton microscopy," Opt. Lett. **23**, 655–657 (1998).
28. T. Minamikawa, M. Hashimoto, K. Fujita, S. Kawata, and T. Araki, "Multi-focus excitation coherent anti-Stokes Raman scattering (CARS) microscopy and its applications for real-time imaging," Opt. Express **17**, 9526–9536 (2009).
29. H. J. Tiziani and H.-M. Uhde, "Three-dimensional analysis by a microlens-array confocal arrangement," Appl. Opt. **33**, 567–572 (1994).
30. A. Orth and K. Crozier, "Microscopy with microlens arrays: high throughput, high resolution and light-field imaging," Opt. Express **20**, 13522–13531 (2012).
31. J. S. George, "Scanning computed confocal imager," U.S. patent 6,038,067 (14 March 2000).
32. D. Toomre and J. B. Pawley, "Disk-scanning confocal microscopy," in *Handbook of Biological Confocal Microscopy*, J. B. Pawley, ed., 3rd ed. (Springer, 2006), pp. 221–238.
33. L. D. Favro, R. L. Thomas, P.-K. Kuo, and L. Chen, "Confocal microscope," U.S. patent 5,162,941 (10 November 1992).
34. K. Isozaki and Y. Kenta Mikuriya, "Confocal microscope," European patent application 1245986 (7 May 1996).
35. S. Hell and R. Pick, "Confocal microscope comprising two microlens arrays and a pinhole diaphragm array," U.S. patent application 20050094261 (3 November 2004).
36. https://readyoptics.com/index_files/Page848.htm
37. P. R. Bevington, *Data Reduction and Error Analysis for the Physical Sciences* (McGraw-Hill, 1969).